Multicellularity, Culture Duration, and Hydrogel Stiffness Guide Induced Pluripotent Stem Cell-Derived Endothelial Progenitor Cell Contractility

Toni M. West,[1] Jiwan Han,[2] Gabriel Peery,[1] Janet Zoldan,[2] and Michael S. Sacks*[,1,2]

[1)] *Willerson Center, Oden Institute for Computational Engineering and Sciences, University of Texas at Austin*

[2)] *Department of Biomedical Engineering, University of Texas at Austin*

(*Electronic mail: msacks@oden.utexas.edu.)

(Dated: 18 June 2025)

Human induced pluripotent stem cells (hiPSCs) offer patient-specific and immune-evasive sources for generating diverse cell types; yet lack of vascularization in hiPSC-derived tissues remains a major limitation for both therapeutic applications and disease modeling. Elucidating the mechanisms underlying vascular network formation in hiPSC-derived cells is therefore imperative. We and others have previously demonstrated that hiPSC-derived endothelial progenitor cells (hiPSC-EPs) self-assemble into lumenized microvascular networks when cultured in 3D norbornene-functionalized hyaluronic acid-based hydrogels. Herein we investigated the early period of culturing to characterize contractility of hiPSC-EPs. We hypothesized that multi-cell cooperativity would increase over time and would be dependent on the original hydrogel storage modulus. To quantify cellular contractility either 4 or 7 days after encapsulation, 3D kinematic analysis was performed on single and small multi-cell clusters of hiPSC-EPs embedded in NorHA-based hydrogels. Contractile responses were significantly and non-linearly influenced by multicellularity, culture duration, and hydrogel stiffness. Novel to this study was the observation that NorHA hydrogels exhibited compressible behaviors, with greater compressibility occurring in NorHA hydrogels with lower stiffness. Hence, the kinematic analysis was modified to incorporate separate deviatoric and volumetric strain indices. At day 7, multicellularity synergistically increased both strain components. These findings indicated that hiPSC-EP contractility and mechanical interactions with the hydrogel are governed by culture duration, multicellularity, and hydrogel stiffness; providing mechanical insight on hiPSC-EP self-assembly into microvasculature networks, a critical step towards development of functional vascular tissues for regenerative medicine and disease models.

I. INTRODUCTION

Human induced pluripotent stem cells (hiPSCs) offer promising untapped patient-specific and immune-evasive cell sources. Therefore, hiPSCs are emerging key players in regenerative medicine and research, not only because they hold the potential to produce a variety of tissue types, but also because of their potential to be engineered for immune compatibility and their potential capacity for large-scale production.[1,2] However, one of the major challenges in clinical translation of hiPSC-based tissue therapies is the lack of vascularization within the derived tissues. This lack of microvasculature in hiPSC-derived constructs has even greater ramification when attempting to repair or study highly vascularized systems that also contain tissue-specific endothelial cells such as heart or brain tissue.[3,4] Therefore, developing hiPSC vascularization techniques will not only improve the efficacy of hiPSC-derived tissues, but it could also become a therapy in and of itself for primarily vascular-related disorders including ischemia, embolism, and diabetic vasculopathy. These challenges underscore the urgent need to deepen understanding of the process of vasculogenesis in hiPSC-derived cells.

Endothelial cells are the main cell type that form capillaries. We and others have developed methods to differentiate hiPSCs into endothelial progenitor (EP) or endothelial cells (ECs), yielding cells with varying levels of maturation and tissue-specific properties depending on the protocol implemented.[5,6] Notably, when hiPSC-EPs are embedded in hyaluronic acid (HA)-based hydrogels and supplemented with vascular endothelial growth factor (VEGF) they undergo morphogenesis to spindle shapes that interconnect with each other to form lumenized structures.[1,7,8] Furthermore, in norbornene-functionalized HA (NorHA) hydrogels cross-linked with varying amounts of enzyme-degradable peptides (EDPs) to produce varying stiffness hydrogels, we found that the more compliant, 190 Pa hydrogels promote the greatest vascular connectivity with longer branch formation and enhanced actin remodeling.[9] In contrast, stiffer (551 Pa) hydrogels have increased mechanotransduction potential as measured by YAP/TAZ nuclear translocation and elevated CD31 endothelial marker expression.[9] These results indicate that hydrogel stiffness affects the vasculogenesis of the hiPSC-EPs as they mature into CD31+ endothelial cells.

However, achieving long-term goals such as developing vascularization strategies for therapy and disease models must be based on an even more detailed understanding of basic mechanodynamics of hiPSC-EPs. We and others have found that cells can profoundly modify their local hydrogel modulus in 3D.[10–13] We and others have also demonstrated that cells actively remodel their extracellular environments by depositing extracellular matrix proteins, such as collagen and laminin, as well as secreting degradation enzymes such as matrix mealloproteinases (MMPs).[5,14–16] Therefore, it is likely that the local mechanical behaviors of NorHA hydrogels will be locally modified by the hiPSC-EPs during culture. Furthermore, other important questions of how multicellularity, hydrogel stiffness, and culturing duration affect hiPSC-EPs' micro-mechanical abilities to produce microvascular networks remain unknown.

As a first step in addressing these questions, the current work focused on characterizing the basal contractile behaviors of EDP-crosslinked NorHA hydrogels of varying stiffness when hiPSC-EPs with differing culture duration and cell numbers were present. This analysis builds upon our previous cell contractile behavior methods[17] to quantify basal contractile displacements and to further define NorHA hydrogel kinematic behaviors that are induced by contracted hiPSC-EPs. It was hypothesized that prior to vascular network formation, multi-cellular cooperativity among hiPSC-EPs would increase hiPSC-EP basal contractility, with these effects evolving over time and being influenced by the shear storage modulus of the 3D hydrogel. By quantitatively analyzing hiPSC-EPs basal contractility, a sizable step forward has been taken in understanding the mechanical cues that drive the development of functional microvasculature structures, paving the way for more effective therapy and research strategies.

II. RESULTS

A. hiPSC-EP Basal Contractile Displacement

To better understand how hiPSC-EPs self-assemble into lumenized networks as they mature within varying stiffness hydrogels, a 3D analysis of single cells and small cell clusters was conducted. The displacements of fluorescent bead fiducial markers embedded in cell-laden hydrogels were tracked before and after treatment with cytochalasin-D (CytoD) so that basal contractility of the cells could be assessed. When comparing initial hydrogel shear storage modulus to the mean contractile displacement of each cellular system, a non-linear relationship existed (Figure 1A-B). As expected, smaller displacements occurred in the stiffer hydrogels, as equal forces applied to a stiffer hydrogel would lead to smaller displacements. For example, in the day 4 single cell conditions, contractile displacement decreased exponentially as the stiffness of the NorHA hydrogel increased (Figure 1A). Small multi-cell clusters exhibited significantly greater basal contractile displacement compared to single cells, especially in more compliant hydrogels (Figure 1A, C). For example, in the 190 Pa hydrogels at day 4, the single cell condition exhibited a 0.5312 μm average contractile displacement, while the multi cell condition average contractile displacement was 1.0210 μm (effect size 0.4898 μm; Figure 1A). Considering that the multi-cell groups are comprised of 2-4 cells, this suggests that although multiple cells basally contracted significantly more than single cells as a group (1A, C, Table I), the overall contractility of each cell diminished.

Extending the cell culture time from 4 days to 7 days further increased basal contractile displacement (Figure 1B-C), with the most pronounced changes occurring in hiPSC-EPs cultured in the most compliant hydrogels. To illustrate, an increase in average contractile displacements of 2.479 μm occurred between day 4 and day 7 for the 190 Pa multi-cell groups (Figure 1B). We have previously determined that during this time period hiPSC-EPs transition into a CD31+ endothelial phenotype with a more developed actin cytoskeleton network.[9] This maturation was associated here with the development of robust mechanisms for basal contractility. Taken together, this data indicates that as cells mature over time in culture, they become significantly more contractile.

When looking at the contractility data overall, initial hydrogel shear storage modulus, cell number, and culture duration each played highly significant roles, both independently and combinatorially, to basal contractile displacements in the hiPSC-EPs (Figure 1C, Table I). Indeed, when these three variables were analyzed together, the change in observed displacements was greater than that explainable by the change in hydrogel storage modulus, suggesting that the hiPSC-EPs modulate their contractility based on the stiffness of their surroundings. While all variables were significant contributors, effect sizes of each factor varied. Initial hydrogel shear storage modulus and culture maturity both had large effects. Multi-cell status had a more modest, although still significant, effect on basal contractile displacements.

B. Volumetric Variations During NorHA Hydrogel Deformation

We and others have previously reported that EDP-crosslinked NorHA hydrogels exhibit swelling behavior.[18,19] This result indicates that the water content in the hydrogels is not entirely bound and thus water transport is possible when deformed, suggesting that they are compressible. In this case the conventional assumption of material incompressibility is no longer valid, and all kinematic analysis must accommodate this fact. We thus first conducted an analysis to determine spatial variations in relative NorHA hydrogel volume changes during basal contraction. This was done by computing the Jacobian $J = det(\mathbf{F})$, where $\mathbf{F}$ is the local deformation gradient tensor (Figure 2; see Methods for details). Note that here J represents the fractional volume change, where $J = 1$ is the incompressible limit. It was noted that in the most compliant, 190 Pa gels that J ranged from less than 0.9 to more than 1.1. This novel finding underscored the compressible nature of the most compliant NorHA Hydrogels induced by cell contraction.

We also found that the spatial variation in J was strongly dependent on initial hydrogel shear storage modulus (Figure 3). Specifically, the 551 Pa Day 4 multi-cell group exhibited the lowest variation in J, having an average J = 1.000 $\pm$ 0.005, and only 0.02% of the mesh elements were where $J \notin [0.95, 1.05]$, indicating nearly incompressible behavior. In contrast, the 190 Pa Day 7 multi-cell samples depicted the largest variation in J, with J = 0.922 $\pm$ 0.056, and 20% of elements were where $J \notin [0.95, 1.05]$, suggesting significant compressibility. An intermediate group, that of the 336 Pa Day 4 multi-cell hydrogels, had an average J = 1.000 $\pm$ 0.009, with 1% of elements being where $J \notin [0.95, 1.05]$. A three-way ANOVA of the standard deviations of J from each sample confirmed that stiffness was a significant contributor to variation in hydrogel volumetric changes (Table I). These results highlight that initial hydrogel stiffness directly impacted local volumetric changes in the hydrogel in a non-linear man-

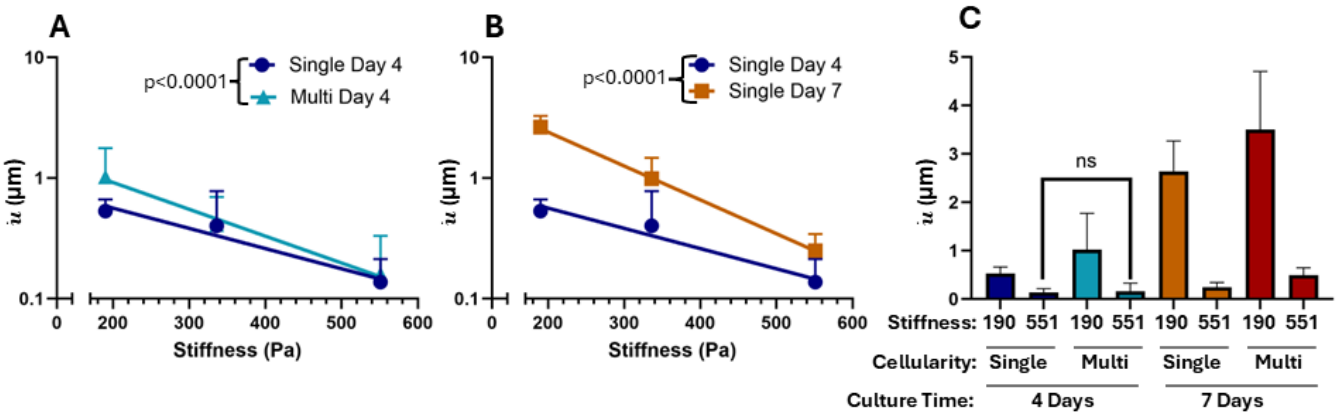

FIG. 1. **Culture duration, cell number, and hydrogel stiffness were significant contributors to cellular contractile displacements.** A-B) Mean ± SEM of cellular contractile displacement plotted against hydrogel stiffness. Non-linear regression analysis was performed implementing a weighted one-phase decay with plateau constrained to 0. A sum of squares F test was then performed to determine significance. A) Multi-cell Day 4 groups exhibited greater contractile displacement ($d(G) = 2.561e^{-0.005125G}$, R^2 = 0.3381) over Single-cell Day 4 groups ($d(G) = 1.218e^{-0.003859G}$, R^2 = 0.3537), with significant difference between the curves (p<0.0001). B) Single-cell Day 7 groups displayed an increased contractile displacement ($d(G) = 8.738e^{-0.006462G}$, R^2 = 0.6412) over Single-cell Day 4 groups, which were significantly different from each other (p<0.0001). C) 3-way ANOVA with Tukey post-test of 190 and 551 Pa samples determined that stiffness, culture time, and cell number all significantly contributed to cellular basal contractile displacement (see Table I for p values). All pairwise comparisons were significant (p<0.0001) except the one marked with "ns" bracket.

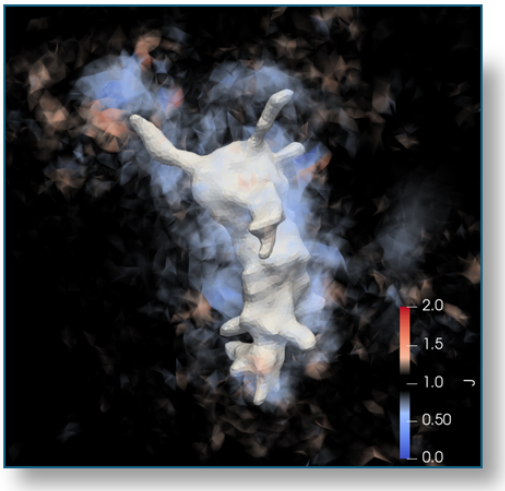

FIG. 2. **NorHA Hydrogels exhibited substantial spatial variations in fractional volume changes.** Representative figure of a 190 Pa NorHA hydrogel containing a multi-cell group cultured for 7 days, showing spatial variations in local hydrogel J values, which ranged from less than 0.9 to more than 1.1.

ner. Since stiffness in these hydrogels was modulated by differing the crosslinker concentration, the hydrogel porosity is concurrently affected, as these properties are intrinsically linked,[20] and is also evidenced by the inverse relationship with the swelling ratio.[18,19] Consequently, porosity may also contribute to the observed variation in J. Given that hydrogel stiffness and the crosslinker concentration exhibited a linear relationship (G(x) = 9.327x - 104.0, R^2 = 0.8851), any mathematical relationship between crosslinker content and variation in J will also hold proportionally to stiffness. Therefore for consistency, stiffness was the representative parameter implemented throughout this study.

The three-way ANOVA performed on the standard deviation of J also depicted that culture duration significantly affected variation in J, both individually and in combination with other variables (Table I). Increased culture duration lead to greater variation in the Jacobian, with the most pronounced effect observed in the most compliant 190 Pa multi-cell group, where the standard deviation of J more than triples from 0.016 on day 4 to 0.056 on day 7 (p<0.0001). Since acellular EDP-crosslinked NorHA hydrogels are stable for weeks,[18] the findings here suggest that the longer the hiPSC-EPs are cultured, the more extensively they can modify their local microenvironment by either increased basal contraction or secretion of extracellular matrix proteins.

Additionally, transitioning from single- to multi-cell groups resulted in a significant increase in the variability of J, with the highest variation observed on day 7 in the most compliant, 190 Pa hydrogels (Table I). In this state, the standard deviation of J nearly doubled from 0.026 in single cells to 0.056 in multi-cell groups (p<0.0001). Again, given that multi-cell samples consisted 2-4 cells, these findings suggest that although the multi-cell systems significantly modify their surroundings more extensively than single cells, the contribution per cell diminishes as additional cells are included. When all the hydrogel compressibility data is considered, the evidence indicates that the hiPSC-EPs modify their hydrogel microenvironment, potentially through either secretory mechanisms or actinomyosin-mediated contractility. This hiPSC-EP-directed modification is highly influenced by culture time, and is more modestly,

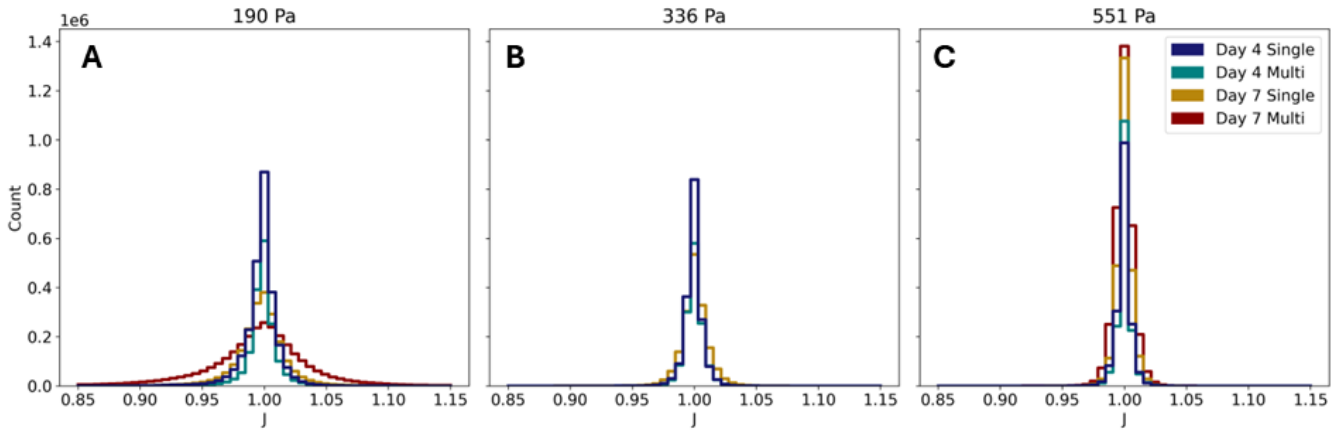

FIG. 3. **Hydrogel deformation varied largely in more compliant NorHA hydrogels.** A-C) Histograms depicting the number of hydrogel finite elements with each J value ranging from J=0.85 to 1.15 per experimental group for A) 190 Pa hydrogels, B) 336 Pa hydrogels, and C) 551 Pa hydrogels.

but significantly, affected by multi-cell status. This is in addition to the increase in variation in J due to initial hydrogel stiffness.

C. Spatial Variations in NorHA Hydrogel Deformation

The observed spatial variations in J led us to investigate whether the local patterns of single cell contractility correlated with local volume changes in the surrounding hydrogel of the most compliant, 190 Pa hydrogels. The hypothesis here was that regions of the hydrogel adjacent to cellular contractile protrusions would undergo tension, while hydrogel areas adjacent to cell zones opposing the contraction would undergo compression. To effectively identify these regions, we analyzed J values corresponding to normalized hydrogel displacements that were either 2 standard deviations above or below the mean (Figure 4). As expected, in regions where the hydrogel was pushed outward, there were significantly lower J values than the contractile regions. However, unexpectedly, the J values in the contractile regions were also significantly lower than 1 ($p<0.0001$ by one-sample T-test). This suggests that even regions under tension undergo measurable compression, highlighting that hydrogel compressibility played a large factor in all areas near the cell.

D. Kinematic Analyses of NorHA Hydrogels During Basal Contraction

Because of the observed significant hydrogel compressibility, the conventional assumption of material incompressibility was no longer valid. Consequently, standard invariant measures of large deformation, such as the first invariant of the right Cauchy-Green deformation tensor, $I_1 = tr(\mathbf{C})$, where $\mathbf{C} = \mathbf{F}^T\mathbf{F}$, had to be modified to account for $J \neq 1$. To address this, deviatoric strain indices were computed. Deviatoric strain represents the component of total strain responsible for change in shape (distortion) independent of volume change. It is the strain that remains after subtracting the hydrostatic strain, which is related to volume change. In essence, deviatoric strain isolates the component of deformation that does not alter its volume.

Thus, for compressible hydrogels I_1 was adjusted to account for the observed volume changes

$$\bar{I}_1 = I_1/J^{2/3} \tag{1}$$

From this relationship, we computed a total deviatoric strain index for the entire hydrogel volume using

$$\mathscr{D}_{dev} = \sum_{elt}^{n} \left[\bar{I}_1^{elt} - 3\right] \tag{2}$$

to quantify the shape-distorting component of the deformation independently of volume effects. Similarly, to account for the total changes in hydrogel volume from cellular contraction, the total volumetric strain index for the entire hydrogel volume was defined as

$$\mathscr{D}_{Vol} = \sum_{elt}^{n} (J^{elt} - 1)^2 \tag{3}$$

When assessing both the deviatoric and volumetric strain indices in relation to hydrogel stiffness, each experimental group exhibited a non-linear trend, with lower initial hydrogel stiffness corresponding to higher strain indices (Figure 5A-B, Figure 5D-E). As expected, larger strain indices occurred in the more compliant hydrogels, which permit greater displacement per unit force. This lead to higher values in both deviatoric and volumetric strain indices. For all experimental groups, linearly reducing initial hydrogel stiffness lead to multi-fold increases in hiPSC-EP-directed strain indices (Figure 5A,B,D,E). Closer examination of the deviatoric strain revealed that multi-cell groups had significantly higher deviatoric strain indices than single cells, with the most pronounced

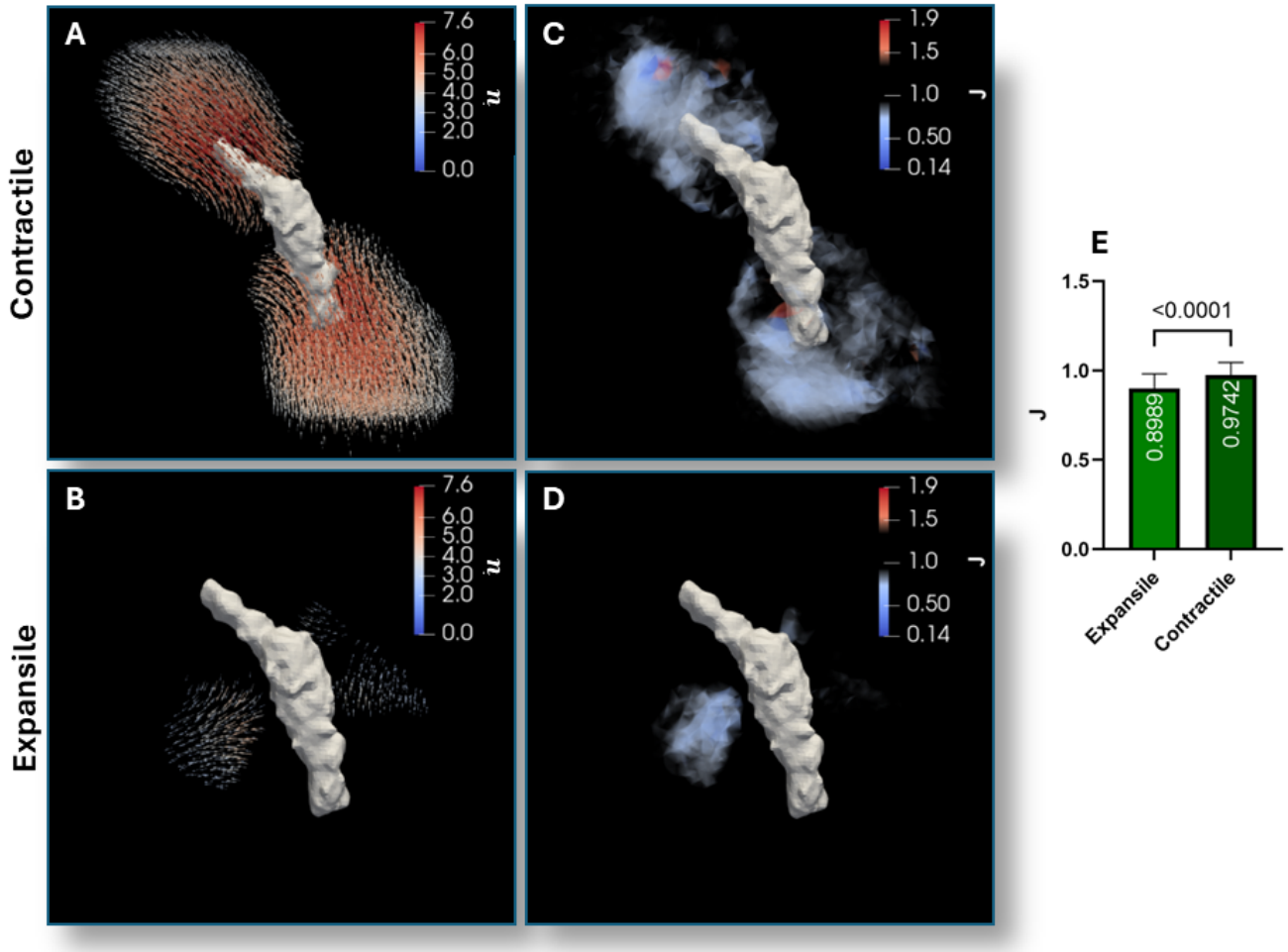

FIG. 4. **Compressibility was more effectual in areas of the hydrogel adjacent to portions of the cell that were expansile.** A-D) Example of a single cell embedded in a 190 Pa NorHA hydrogel with displacements A) 2 standard deviations above and B) 2 standard deviations below the mean displacement of the hydrogel, C-D) which were correlated with the Jacobians, J, in the same locations. E) Welch's unpaired two-tailed T-test of Jacobians seen in C and D. Mean $\pm$ standard deviation depicted as bars with values and error bars. p value indicated in bracket.

difference observed in the more compliant hydrogels (Figure 5A, Table I). Although differences in deviatoric strain due to multicellularity on day 4 were modest, by day 7, a synergistic effect emerged between single- and multi-cell samples. For instance, in 190 Pa hydrogels on day 7, single cells had an average deviatoric strain index of 18724, while multicellular samples demonstrated a significantly higher average deviatoric strain index of 78449 .

As mentioned above, culture duration further amplified the hiPSC-EP-generated changes in strain indices. For example, in the 190 Pa single cell hydrogels, the deviatoric stain index increased by 14669 between day 4 and 7 (Figure 5B-C). This, in conjunction with the three-way ANOVA results (Table I), illustrated that culture duration largely and significantly affected deviatoric strain index. In summary, the three-way ANOVA confirmed that stiffness, multicellularity, and culture duration were all significant contributors, both alone and in combination, to the deviatoric strain index (Figure 5C, Table I). These findings indicate that hiPSC-EPs induce shape changing strains on their surroundings during basal contractility, and that the cells were significantly influenced by initial hydrogel stiffness, multicellular status, and culture duration.

For volumetric strain index, day 4 data depicted no significant differences between single- and multi-cell groups across stiffness levels, with data fitting a single curve (Figure 5D). However, by day 7, a three-way ANOVA revealed that cell number significantly affected volumetric strain index both independently and in combination with hydrogel stiffness and culture duration. A Tukey post-test denoted a significant difference between single and multi-cell groups on Day 7 in the most compliant, 190 Pa hydrogels (Figure 5F, Table I). The affect size for these day 7 samples is as much as 11.15 times larger in 190 Pa hydrogels, depicting that multicellularity plays a pivotal role that becomes synergistic over time

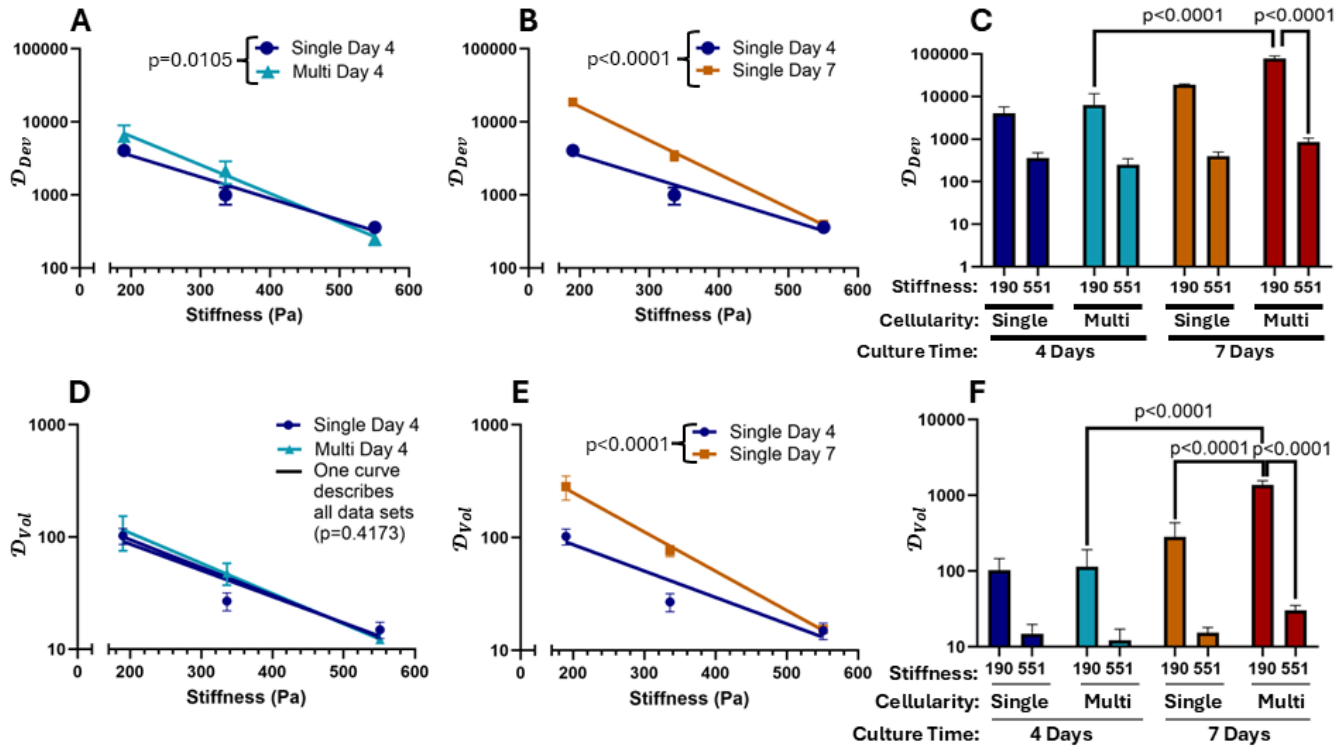

FIG. 5. **Culture duration, cell number, and hydrogel stiffness were significant contributors to deviatoric strain index and, to a lesser extent, volumetric strain index.** A-B, D-E) Mean ± SEM of indicated average strain index per group plotted against hydrogel stiffness. Non-linear regression analysis was performed implementing a weighted one-phase decay equation with plateau constrained to 0. Significance between data sets was assessed via a sum of squares F test. C, F) 3-way ANOVA with Tukey post-test of 190 and 551 Pa hydrogels for indicated strain indices (see Table I for p values). Significant single variable comparisons depicted with brackets. A) Multi-cell Day 4 groups had an increased deviatoric strain in more compliant hydrogels ($\sigma(G) = 38685e^{-0.009019G}$, R^2 = 0.6312) compared to Single-cell Day 4 groups ($\sigma(G) = 13381e^{-0.006758G}$, R^2 = 0.7431), with significant difference between the groups (p=0.0105). B) Single-cell day 7 groups had significantly greater deviatoric strain ($\sigma(G) = 134931^{e-0.01062G}$, R^2 = 0.9178) over Single-cell day 4 groups, which were significantly different from each other (p<0.0001). C) Stiffness, culture time, and cell number all significantly contributed to deviatoric strain index. D) Single and Multi-cell Day 4 groups had data that could be sufficiently described by one best fit curve ($\sigma(G) = 297.2e^{-0.005707G}$, R^2 = 0.6632, p=0.4173) with no significant difference between groups. E) Single-cell day 7 groups had an increased volumetric strain index ($\sigma(G) = 1245e^{-0.008017G}$, R^2 = 0.8075) over single-cell day 4 groups ($\sigma(G) = 254.0e^{-0.005390G}$, R^2 = 0.6819), which were significantly different from each other (p<0.0001). F) Stiffness, culture time, and cell number all significantly contributed to volumetric strain index.

for hiPSC-EP-mediated hydrogel volume modulation during basal contraction.

Comparison of regression equations representing single cell volumetric strain indices with respect to stiffness from Day 4 and Day 7 revealed a significant difference in volumetric strain index because of culture duration, which was confirmed by three-way ANOVA (Figure 5E-F, Table I). In more compliant hydrogels, the increase in volumetric strain index was pronounced, having an affect size of 12.05 times greater on day 7 than on day 4. This information indicates that culture duration significantly impacts the hydrogel's volumetric strain index, possibly due to the hiPSC-EPs having more time to modify their local environments through secretion of degradation enzymes such as MMPs.[5,14–16] When comparing the deviatoric strain indices to the volumetric strain indices, the differences in value were largely skewed to higher deviatoric strain index values, with an average effect multiplier of 39.61 ± 17.64. This indicates that the deviatoric portion of strain dominates the cell-hydrogel interaction by a factor of 40. Taken together with the above reported variation in Jacobians, it is evident that the volumetric strain index is not inconsequential, albeit relatively small compared to that of the deviatoric strain index. Therefore, volumetric strain must be accounted for in hydrogel systems such as the cross-linked NorHA hydrogels to accurately characterize their mechanical behavior and deformation kinematics.

To further determine how strain indices play a role in hiPSC-EP function, an element-wise spatial analysis was performed of deviatoric strain index and volumetric strain index. This analysis revealed that the hydrogel elements in close proximity to the cellular surface exhibited the largest values for both deviatoric strain and volumetric strain. Indeed, elements in the 99th percentile or higher are consistently associated with the cellular surface across all groups (Figure 6,

Figure 7). Moreover, the same elements that had high deviatoric strain indices also had high volumetric strain indices. This suggests that basal contractile forces exerted by the cells played a major role in driving these localized deformations.

Another notable trend that emerges from the spatial analysis of strain indices is that there was at least one protrusion per cell or cell cluster that lacked any of the highest strain values (see arrows on Figures 6 and 7). This data may reflect on the migratory behavior of the hiPSC-EPs. hiPSC-EPs may be migrating as observed previously in fibroblasts where inhibiting or knocking down MMPs lead to a decrease in leading edge migratory behavior.[21] MMP degradation of the hydrogel inside the elements near the leading edge of hiPSC-EPs may be indicated here by areas of high differentials in strain indices. On the other end, lagging tail migratory dynamics are dominated by myosin kinetics inside the cell,[22] and therefore lagging tails are not likely to hydrolytically modify their immediate surroundings. This observation may suggest that the portion of the cell that has little matrix modification around it may be the lagging tail. That this phenomenon occurred in both single cells and multi-cell clusters further supports the possibility that groups of hiPSC-EPs may migrate collectively through a process known as plithotaxis, where cells within a cluster align along the direction of maximal principal stress, a behavior previously reported in endothelial cells in a variety of 2D settings[23].

III. DISCUSSION

A. Findings

Our long-term goal is to understand how hiPSC-EPs modify their surroundings as they form lumenized networks in 3D crosslinked NorHA hydrogels, ultimately designing angiogenic biomatrices that induce superior microvascularization in hiPSC-derived cellular constructs. As a step in this process, the current study focused on the transition from single cells to small multi-cell clusters in the early days after hiPSC-EP embedding. It was found that not only did hydrogel stiffness, culture duration, and cell number significantly affect basal contractile displacement magnitude, but they also contribute significantly to the compressibility of the crosslinked NorHA hydrogel. Specifically, more compliant hydrogels and increased time in culture or number of cells per cluster led to greater observed volume changes in the hydrogel, indicating enhanced compressibility. To account for these volume changes, a kinematic analysis separating the deviatoric and volumetric terms of strain was completed. Both the deviatoric and volumetric strain indices were significantly affected by hydrogel stiffness, culture duration, and multicellularity, with the deviatoric strain index having a substantially larger effect size than the volumetric strain index.

An interesting outcome of this study was that the crosslinked NorHA hydrogels were substantially modified by the embedded hiPSC-EPs. This is evident across all parameters assessed. It is well known that cells embedded in hydrogels secrete copious amounts of extracellular matrix proteins and degradation enzymes,[5,14–16] and that they pull on their surroundings through basal contraction.[24,25] Several studies have portrayed that local and/or bulk hydrogel shear moduli can be modified by cells in various non-NorHA hydrogels.[10,14–16] But until now there was not a full 3D micron-level investigation into how acutely scalar deformation indices in the hydrogel would be affected by hiPSC-EPs growing in crosslinked NorHA hydrogels. Most work associated with steady-state material models of NorHA hydrogels assumes that they are incompressible or nearly incompressible[26–28] even though swelling behavior has been previously outlined in these hydrogels.[18,19] In previous 3D strain mapping studies of sprouting angiogenesis in endothelial cells, EDP-crosslinked poly(ethylene) glycol (PEG) hydrogels were modeled using a linear elastic model to quantify basal traction forces of the sprouting cells, but neither the possibility that the hydrogel was inherently compressible nor the potential for enzyme degradation occurring in the hydrogel were thoroughly addressed.[29,30] Indeed, in a variety of cell types and hydrogels where detailed 3D strain mapping techniques have been implemented, compressibility is at most accounted for by instituting the deviatoric invariants in their calculations, but no further pursuit of the matter of compressibility is undertaken.[31–34] Therefore, to the best of our knowledge, the present work is the first to portray in detail how varying culture conditions such as hydrogel stiffness, time, and cell number differentially affect sub-micron changes in a hydrogel's scalar deformation indices in full 3D.

One key hypothesis for this study was that multi-cellularity would amplify the effects of hydrogel stiffness and culture duration on hiPSC-EP basal contractility and cell-mediated hydrogel modification. In day 4 cultures, multicellularity significantly increased most investigated parameters but did not impart clear synergistic effects. By day 7, however, synergism became apparent in both deviatoric and volumetric strain indices. Although cell clusters in this study were limited to 2-4 cells, the data suggest that even small clusters can drive collective matrix and cytoskeletal remodeling over time. These effects are likely due to multicellular hiPSC-EP groups secreting larger amounts of degradation enzymes in combination with higher overall actinomyosin activity. We have previously described that MMP-1 and MMP-13 significantly decrease the stiffness of NorHA-based hydrogels,[5] making these prime candidates for future investigations of hiPSC-EP-mediated hydrogel degradation on the micro-scale. Furthermore, the extended 7-day culture duration likely provided increased time for modification of the hydrogel and production of more robust cytoskeletal structures, contributing to the larger observed shape deformations. Notably, we have previously seen that hiPSC-EP cytoskeletal remodeling is especially strong in more compliant hydrogels,[9] which aligns with our current findings where the largest deviatoric strain indices are observed in the most compliant hydrogels after 7 days of culture.

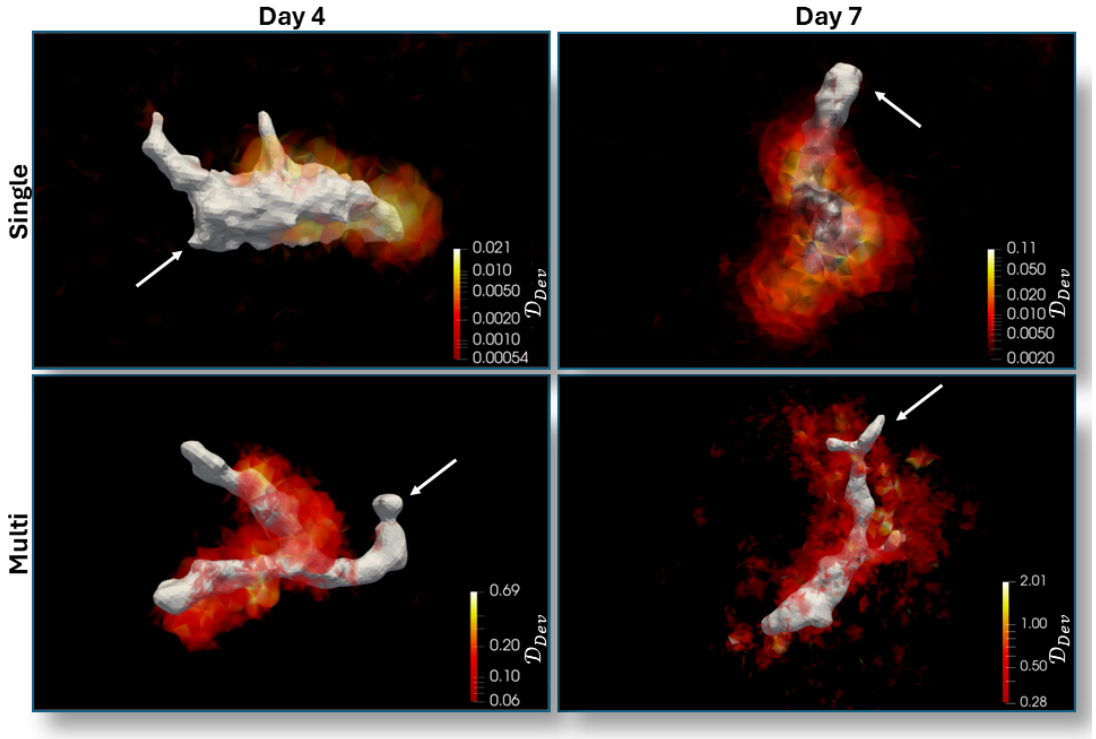

FIG. 6. **Largest deviatoric strain indices concentrated near cells but exhibited minimal overlap with at least one protrusion.** 99th percentile and higher of deviatoric strain indices of representative hydrogels depicted in each rendering with marked values in respective scale bars. Arrows illustrate a protrusion in each image where high deviatoric strain indices were notably absent.

B. Study limitations

Herein it can be seen that local kinematic parameters of the EDP-crosslinked NorHA hydrogels are significantly modified by embedded hiPSC-EPs. This information is consistent with our previous work and others' illustrating that hiPSC-EPs deposit extracellular matrix proteins such as collagen and laminin that differ in mechanical properties distinct from the native hydrogel. Simultaneously, hiPSC-EPs secrete matrix metalloproteinases (MMPs) which facilitate matrix degradation and support cell growth into their surrounding space.[5,14–16] Induced heterogeneous modifications of NorHA hydrogel moduli by these processes were unknown, thus direct calculation of the cell-generated traction forces was not feasible. However, we have developed a method to determine local moduli of poly(ethylene) glycol-based hydrogels,[10] which we are now adapting for this dataset to enable precise assessment of both hiPSC-EP traction forces during basal contractility and hiPSC-EP-directed modification of their microenvironment over time which will greatly clarify and delineate the differing contributions of cell secretion and actinomyosin activity to the overall basal contractile behavior of the hiPSC-EPs as they form networks.

The present investigation was limited to exploring the transition of hiPSC-EPs from the fully relaxed, CytoD-treated steady state to the basal steady state so that basal tonus could be determined. This limitation was imposed by the time constraints associated with acquiring high resolution full 3D images of the cells and hydrogels. The collected data demonstrate that the more compliant crosslinked NorHA hydrogels became compressible, with degree thereof increased over culture time of embedded hiPSC-EPs. Since by-the-minute measurements could not be recorded during cell relaxation, time-dependent models of the NorHA hydrogel properties could not be explored. Previous work has assumed that EDP-crosslinked NorHA hydrogels behave as incompressible neo-Hookean materials under steady state conditions[26] , consistent with the behavior in many other hydrogel steady state systems.[35,36] Additionally, the porosity of cell-free NorHA hydrogels is well characterized[20] and hydrogels have been seen to have poroelastic properties when measured over relevant time scales.[37–39] Therefore, dynamics of the water portion of the hydrogel through its porous structure may be the primary mechanism for the observed compressibility during hiPSC-EP basal contraction.[40–42] Recent advances in light sheet confocal microscopy have greatly improved the speed at which highly-precise full-3D imaging can be performed.[43] As this technology becomes more readily available, illumination of time-dependent mechanisms of 3D hydrogel dynamics in cellularized conditions will be forthcoming.

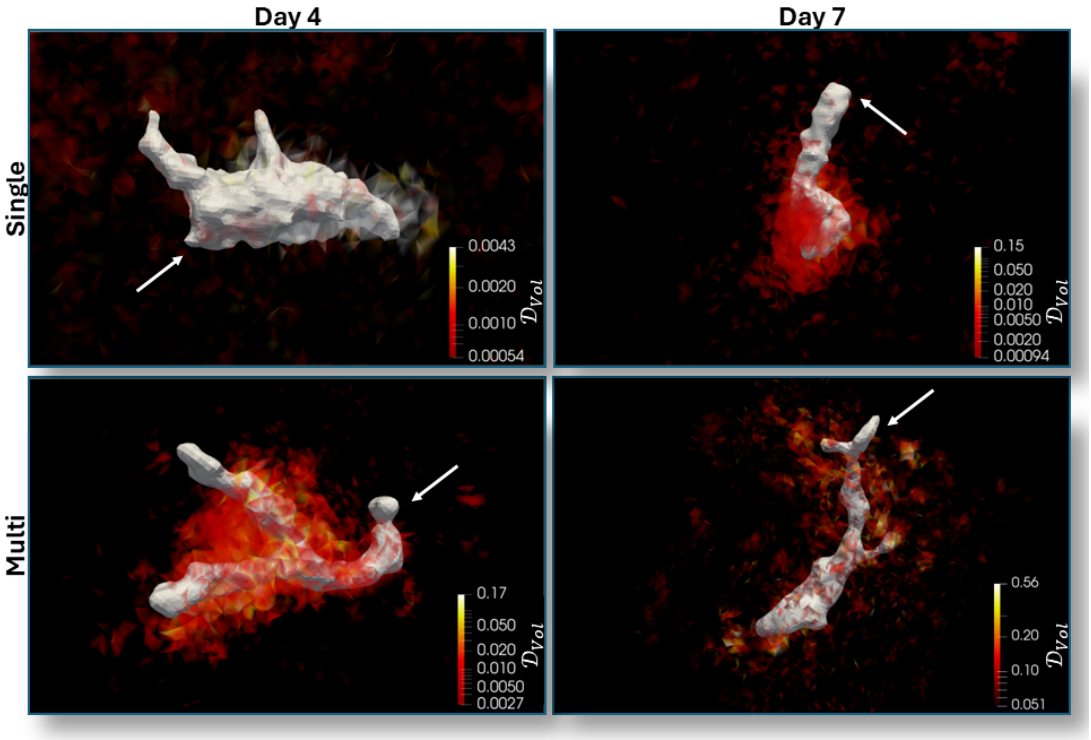

FIG. 7. **Largest volumetric strain indices also concentrated near cells and exhibited minimal overlap with the same protrusion.** 99th percentile and higher of volumetric strain indices of representative hydrogels depicted in each rendering with marked values in respective scale bars. Arrows illustrate a protrusion in each image where high volumetric strain indices were notably absent.

C. Conclusions

We have established that key environmental conditions can significantly affect cell-mediated changes in hydrogel properties on a micro-environmental scale. Namely, the local Jacobians reveal that EDP-crosslinked NorHA hydrogels become more compressible near hiPSC-EPs, with this effect strongly dependent on initial hydrogel stiffness, culture duration, and multicellularity. Furthermore, both volumetric and deviatoric strain indices are also significantly dependent on these attributes of the 3D culture. Further work quantifying these differences will allow for an accurate calculation of traction forces and will provide deeper insight of the biomechanical processes by which hiPSC-EPs self-assemble into interconnected lumenized networks. These insights will inform the development of angiogenic biomaterials that drive effective vascularization strategies in hiPSC-derived tissue constructs.

IV. METHODS

A. Summary of Approach

In the present study we sought to determine the contractile behavior of hiPSC-EPs in 3D hydrogel cultures as they begin to self-assemble into capillary-like structures by performing a detailed 3D strain mapping analysis of these cells (Figure 8). hiPSCs that stably express tdTomato were differentiated into EPs and embedded in norbornene-functionalized hyaluronic acid (NorHA) hydrogels containing fluorescent microbead fiducial markers and cross-linked with enzyme-degradable peptides (EDP) of different percentages to produce varying stiffnesses. hiPSC-EPs were then imaged either 4 or 7 days after encapsulation. With added filtering steps to avoid erroneous bead tracking, the FM-TRACK software we previously published[17] was deployed to track the movements of the cell and hydrogel due to basal contractility. Additionally, new software was written in Python to analyze the kinematic parameters of the system which implemented deviatoric and volumetric divisions of strain indices.

B. Differentiation and Gelation of 3D Endothelial Progenitor Cells (EPs)

hiPSCs stably expressing tdTomato (WiCell) were differentiated into EPs as previously described by Jalilian et al.[44] and us.[5] On day 5 of differentiation, cells were sorted for EP marker, CD34. Sorted cells were embedded in NorHA hydrogels containing Dragon green 0.51 μm diameter beads (Bangs Labs) as described in detail in Han et al.[9] Three types of

3-Way ANOVA p Values

	σ_J	$\bar{u}_{Cell}$	$\bar{\mathscr{D}}_{Dev}$	$\bar{\mathscr{D}}_{Vol}$
Stiffness	<0.0001	<0.0001	<0.0001	<0.0001
Day	<0.0001	<0.0001	<0.0001	<0.0001
Cell Number	0.0010	<0.0001	0.0001	0.0004
Stiffness & Day	<0.0001	<0.0001	<0.0001	<0.0001
Stiffness & Cell Number	0.0028	<0.0001	0.0001	0.0005
Day & Cell Number	0.0011	<0.0001	0.0003	0.0005
Stiffness & Day & Cell Number	0.0050	<0.0001	0.0004	0.0006
Single Variable Comparisons:				
	190 Multi Day 4 vs Day 7 <0.0001			190 Multi Day 4 vs Day 7 <0.0001
	190 Day 7 Single vs Multi <0.0001	All combos significant <0.0001	190 Multi Day 4 vs Day 7 <0.0001	Day 7 Multi 190 vs 551 <0.0001
	Day 7 Multi 190 vs 551 <0.0001	except 551 Day 4 Single vs Multi 0.4019	190 Day 7 Single vs Multi <0.0001	190 Day 7 Single vs Multi <0.0001

TABLE I. **Culture duration, cell number, and hydrogel stiffness are significant contributors to the variation in hydrogel deformation, average cellular contractile displacements, average deviatoric strain index, average volumetric strain index, and average total strain index.** Independent variables for all 3-way ANOVAs with Tukey post-test were kept as culture duration (Day 4 vs Day 7), cell number (Single vs. Multi), and hydrogel stiffness (190 Pa vs 551 Pa). p values for each variable comparison to the indicated dependent variable are tabulated, followed by a listing of all relevant significant p values for single independent variable comparisons.

hydrogels were produced with varying concentrations of the enzymatically degradable peptide (EDP) KCGPQGIWGCK, with 25%, 50%, and 75% cross-linked hydrogels having concentrations of 1.458 mM, 2.916 mM and 4.357 mM of EDP, respectively. As we reported,[9] it was found that hydrogels with 25% crosslinker had a stiffness of 190 $\pm$ 33.3 Pa, the 50% hydrogels had a stiffness of 336 $\pm$ 67.4 Pa, and the 75% hydrogels had a stiffness of 551 $\pm$ 90.1 Pa. Cell-laden hydrogels were cultured in EGM-2 media supplemented with 50 ng/mL VEGF165 and 10 μM Y-27632 for the first 24 hours and were changed daily thereafter with EGM-2 media for either 4 or 7 days.

C. 3D Cell Contractile Behavior Imaging

3D contractile-behavior imaging was performed on single cells and small multi-cell groups that fully fit in the microscope field of view from hiPSC-EP-laden hydrogels cultured for either 4 or 7 days, as we have previously described[45] with the following improvements. Immediately prior to imaging, the embedded hiPSC-EPs were stained for 30 minutes in Hoecht following manufacturer directions. Then, 2.9 mL of phenol-free media was placed in the dish. Images were taken with a 40x silicone oil objective lens on a Nikon AXR confocal equipped with a Tokai hit stage incubator set to 37°C and a Queensgate NanoScan SP Z Series Piezo. This system is housed at the Center for Biomedical Research Support Microscopy and Flow Cytometry Facility at the University of Texas at Austin (RRID: SCR_021756). Lasers of 405 nm, 488 nm, and 561 nm were simultaneously emitted onto the sample for imaging the cell nuclei, dragon-green fiducial marker beads, and the tdTomato-expressing hiPSC-EPs in a 147x147x119.23 μm field of view (FOV) with isotropic voxels of side length 0.288 μm that had been corrected for spherical aberration. Single cells or multi-cell groups were identified by the number of nuclei that were associated with the tdTomato-expressing portions of the image. After hiPSC-EPs were imaged in their basal states, 100 μL of 120 μM of the potent actin polymerization inhibitor, cytochalasin-D (CytoD, MilliporeSigma) was added to achieve a final concentration to 4 μM. After 40 minutes of CytoD treatment at 37 °C, the same FOV was then re-imaged with the cells in the fully-relaxed steady state.

D. Image Processing, Mesh Production, and Displacement Analysis

After converting each color channel of the 3D image into individual 8-bit-tiff slice images in ImageJ-Fiji (Fuji), Python software was implemented to segment and generate high fidelity finite element (FE) meshes of the red fluorescence images of the cells in the CytoD steady state. This Python code was designed with tunable parameters so that masking and meshing could accurately capture the true 3D cellular structure. Specifically, the scikit image library[46] performed salt & pepper removal, small hole filling, Gaussian blurring, manual thresholding, curvature-driven diffusion, and binary closing with default parameters, and then augmentations to the defaults were made to produce a congruent mask. Similarly, the pymeshlab library[47] performed lewiner marching cubes, taubin smoothing, T-verticies removal, hole closing, and setting the mean element side length to 0.5 μm, which resulted in highly accurate FE mesh representations of cellular geometry (Figure 8).

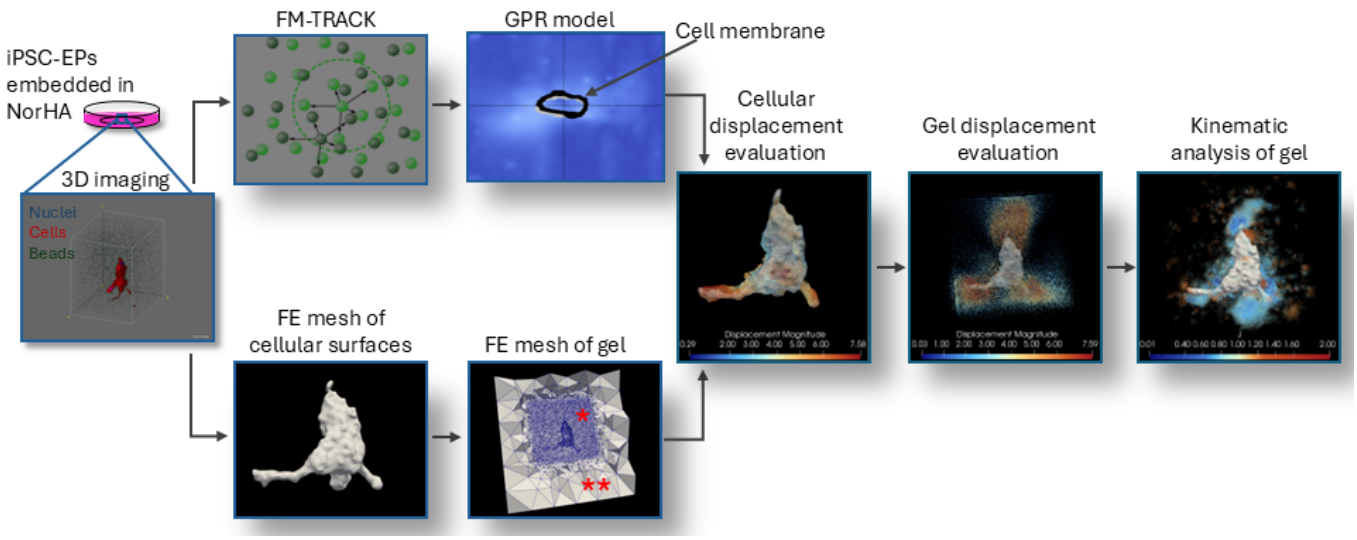

FIG. 8. **Pipeline for Experimentation and Analysis.** Schematic overview of the experimental and analytical workflow implemented to produce the presented data. Induced pluripotent stem cell-derived endothelial progenitor cells (hiPSC-EPs) were embedded in norbornene-functionalized hyaluronic acid hydrogels (NorHA) containing green fluorescent beads which were cultured for 4 or 7 days. Samples were imaged via 3D confocal microscopy under both basal and cytochalasin-D-treated states. FM-TRACK software[17] analyzed the position and displacement of the beads in the hydrogel, and a Gaussian process regression (GPR) model was constructed to represent displacements throughout the system. The blue channel was evaluated to quantify cell number and the red channel was utilized to produce a finite element (FE) surface mesh of the cells. A corresponding hydrogel finite element (FE) mesh was then made with the imaged region meshed at average edge lengths of 2.86 μm and the surrounding extrapolated region had increasing side lengths from 2.86 μm up to 50 μm. Displacements were then mapped onto the nodes of the cell and hydrogel meshes, and a kinematic analysis of the hydrogel was completed.*Imaged region, ** Extrapolated region.

The green fluorescence images were processed with the FM-TRACK software we have previously described,[17] which tracks the movement of the fiducial marker beads embedded in the hydrogel going from the fully-relaxed, CytoD-treated steady state to the basal state so that basal contractility can be assessed. Rigid body motion caused by microscope stage movement was corrected for with multivariate adaptive regression splines[48] and then spurious beads were filtered out. A Gaussian process regression (GPR) model[48] of the cell/hydrogel displacements was fit to resultant bead displacement vectors and locations. Displacements were then interpolated onto the cell surface FE mesh to establish a direct one-to-one correspondence between the fully-relaxed steady state of cells and their basally-contracted state. To assess the direction of contractile displacement relative to the surface of the cell, signed displacement magnitudes were computed by multiplying displacement magnitudes by the dot product of unit vectors pointing radially outward from the cell center with nodal cellular displacement vectors. Then, negative values represented displacements moving in towards the center of the cell and positive values represented displacements moving away from the center of the cell. To graph contractile response, the normalized displacements were multiplied by -1 to make contractile events positive, and then a threshold of 0 was set to isolate contractile regions.

For analyzing the kinematic parameters of the NorHA hydrogels, a finite element (FE) mesh of each hydrogel was generated with Gmsh python library functions.[49] The center of the hydrogel mesh was defined as the centroid of the cell surface FE mesh. A multi-tiered bounding box approach was employed to produce the hydrogel mesh, producing a computationally tractable model with uniform dimensions for all cells that encompassed a larger volume than could be visualized in the microscope FOV. The inner-tier box represented the experimentally-imaged FOV around the cell, while the outer-tier box represented extrapolated readouts of what occurs in the hydrogel 150 μm from the cell centroid (Figure 8). The element side lengths from the cell surface to the edge of the inner bounding box were set to average 2.86 μm. This characteristic side length was determined from an exemplar cell to balance geometric fidelity and computational efficiency. Implementing similar methods, the element side lengths between the inner and outer bounding boxes were set to increase exponentially from 2.86 μm to 50 μm. The cell itself was modeled as a hollow inclusion in the center of the hydrogel.

To determine displacements independent of fiducial bead placement and to accurately capture the local displacement field at any location in the FE mesh for each hydrogel, the GPR model produced from the fluorescent-green-bead displacements was evaluated at each node of the hydrogel FE mesh. The directions of signed displacement vectors were normalized to the cell centroid as described above to ensure consistent directional interpretation. The resulting normalized displacements were then parsed by standard deviation of displacement magnitudes throughout the hydrogel to evaluate the spatial distribution of contractile vs. expansile regions of the

cell (Figure 4).

E. Hydrogel Deformation Analysis

Because the hydrogel may have properties of a compressible solid, an assessment of the deformation behavior of the NorHA hydrogel was performed by calculating the Jacobian determinant, which quantifies local volumetric changes. The deformation gradient was given by $\mathbf{F} = \mathbf{I} + \nabla\mathbf{u}$ for each element in a given hydrogel mesh, where $\mathbf{I}$ is the identity tensor and $\nabla\mathbf{u}$ is the displacement gradient tensor. This was computed in Python according to the constant strain tetrahedron approach, multiplying the matrix of relative displacements between the nodes of a tetrahedron by the inverse of the matrix of relative reference positions. The right Cauchy-Green deformation tensor was then calculated as $\mathbf{C} = \mathbf{F}^T\mathbf{F}$, and the Jacobian determinant was defined as $J = \det(\mathbf{F})$.

Visualizations were generated in Paraview 5.13.2 (Kitware), histograms were prepared in Python, and graphs and statistics were produced on Prism 10.3.0 (GraphPad). A value of $p<0.05$ was considered significant. Implemented statistical tests are delineated in each figure legend. Unless otherwise stated, all materials were acquired from Thermo-Fisher Scientific.

V. ACKNOWLEDGMENTS

TMW is an NIH F32 post-doctoral fellow (1F32HL167570). This work is graciously funded by the following grant awards: NIH-R01EB032533, NIH-R01HL157829, and UTAUS-FA00000461.

Author Contributions: TMW: data curation (lead), formal analysis (lead), funding acquisition (equal), investigation (equal), methodology (equal), project administration (supporting), software (lead), validation (lead), visualization (lead), writing/original draft preparation (lead). JH: data curation (supporting), investigation (equal), methodology (equal). GP: formal analysis (supporting), software (supporting), visualization (supporting), writing/review & editing (supporting). JZ: conceptualization (equal), formal analysis (supporting), funding acquisition (equal), methodology (equal), project administration (equal), resources (lead), supervision (equal), writing/review & editing (equal). MS: conceptualization (equal), formal analysis (supporting), funding acquisition (equal), methodology (equal), project administration (lead), resources (lead), supervision (lead), writing/review & editing (equal).

VI. DATA AVAILABILITY STATEMENT

The data that support the findings of this study are available from the corresponding author upon reasonable request.

VII. CONFLICT OF INTEREST STATEMENT

The authors declare no conflicts of interest.

VIII. ETHICS STATEMENT

All experiments were carried out in accordance with the University of Texas at Austin regulations and NIH guidelines.

IX. HIGHLIGHT IMAGE

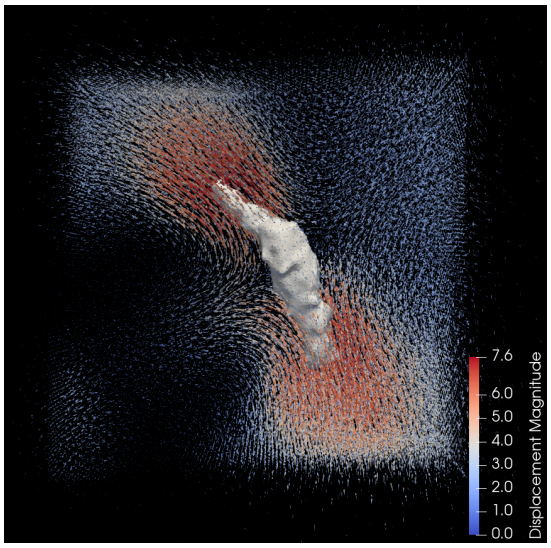

FIG. 9. **Highlight Image**

[1] K. E. Martin, Q. Hammer, K. Perica, M. Sadelain, and K.-J. Malmberg, "Engineering immune-evasive allogeneic cellular immunotherapies," Nature Reviews Immunology **24**, 680–693 (2024).

[2] X. Shi, K. Zhang, F. Yu, Q. Qi, X. Cai, and Y. Zhang, "Advancements and innovative strategies in induced pluripotent stem cell-derived mesenchymal stem cell therapy: A comprehensive review," Stem Cells International **2024**, 4073485 (2024), https://onlinelibrary.wiley.com/doi/pdf/10.1155/2024/4073485.

[3] C. Liu, D. Han, P. Liang, Y. Li, and F. Cao, "The current dilemma and breakthrough of stem cell therapy in ischemic heart disease," Frontiers in Cell and Developmental Biology **Volume 9 - 2021** (2021), 10.3389/fcell.2021.636136.

[4] J. Cerneckis, H. Cai, and Y. Shi, "Induced pluripotent stem cells (iPSCs): molecular mechanisms of induction and applications," Signal Transduction and Targeted Therapy **9**, 112 (2024).

[5] B. Stern, S. Meng, B. Larsen, A. Brock, and J. Zoldan, "Differentiation Protocol-Dependent variability in hiPSC-Derived endothelial progenitor functionality," Regenerative Engineering and Translational Medicine (2025).

[6] J. Nguyen, Y.-Y. Lin, and S. Gerecht, "The next generation of endothelial differentiation: Tissue-specific ECs," Cell Stem Cell **28**, 1188–1204 (2021).

[7] C. O. Crosby and J. Zoldan, "Mimicking the physical cues of the ecm in angiogenic biomaterials," Regenerative Biomaterials **6**, 61–73 (2019), https://academic.oup.com/rb/article-pdf/6/2/61/28269574/rbz003.pdf.

[8] C. O. Crosby, D. Valliappan, D. Shu, S. Kumar, C. Tu, W. Deng, S. H. Parekh, and J. Zoldan, "Quantifying the vasculogenic potential of induced

pluripotent stem cell-derived endothelial progenitors in collagen hydrogels," Tissue Engineering Part A **25**, 746–758 (2019), pMID: 30618333, https://doi.org/10.1089/ten.tea.2018.0274.

[9]J. Han, K. Halwachs, T. West, B. Larsen, M. S. Sacks, A. M. Rosales, and J. Zoldan, "Matrix stiffness regulates mechanotransduction and vascular network formation of hipsc-derived endothelial progenitors encapsulated in 3d hydrogels," bioRxiv (2025), 10.1101/2025.04.11.648340, https://www.biorxiv.org/content/early/2025/04/30/2025.04.11.648340.full.pdf.

[10]A. Khang, J. Steinman, R. Tuscher, X. Feng, and M. S. Sacks, "Estimation of aortic valve interstitial cell-induced 3d remodeling of poly(ethylene glycol) hydrogel environments using an inverse finite element approach," Acta Biomaterialia **160**, 123–133 (2023).

[11]B. A. Juliar, J. A. Beamish, M. E. Busch, D. S. Cleveland, L. Nimmagadda, and A. J. Putnam, "Cell-mediated matrix stiffening accompanies capillary morphogenesis in ultra-soft amorphous hydrogels," Biomaterials **230**, 119634 (2020).

[12]E. Kniazeva, J. W. Weidling, R. Singh, E. L. Botvinick, M. A. Digman, E. Gratton, and A. J. Putnam, "Quantification of local matrix deformations and mechanical properties during capillary morphogenesis in 3d," Integrative Biology **4**, 431–439 (2012), https://academic.oup.com/ib/article-pdf/4/4/431/27320888/c2ib00120a.pdf.

[13]B. A. Juliar, M. T. Keating, Y. P. Kong, E. L. Botvinick, and A. J. Putnam, "Sprouting angiogenesis induces significant mechanical heterogeneities and ecm stiffening across length scales in fibrin hydrogels," Biomaterials **162**, 99–108 (2018).

[14]A. Hartley, P. M. Williams, and A. Mata, "A comparison of the mechanical properties of ecm components and synthetic self-assembling peptides," Advanced Healthcare Materials **n/a**, 2402385 (2025), https://advanced.onlinelibrary.wiley.com/doi/pdf/10.1002/adhm.202402385.

[15]N. R. Ariyasinghe, R. de Souza Santos, A. Gross, A. Aghamaleky-Sarvestany, S. Kreimer, S. Escopete, S. J. Parker, and D. Sareen, "Proteomics of novel induced pluripotent stem cell-derived vascular endothelial cells reveal extensive similarity with an immortalized human endothelial cell line," Physiological Genomics **55**, 324–337 (2023), pMID: 37306406, https://doi.org/10.1152/physiolgenomics.00166.2022.

[16]K. Goodarzi and S. S. Rao, "Structurally decoupled hyaluronic acid hydrogels for studying matrix metalloproteinase-mediated invasion of metastatic breast cancer cells," International Journal of Biological Macromolecules **277**, 134493 (2024).

[17]E. Lejeune, A. Khang, J. Sansom, and M. S. Sacks, "Fm-track: A fiducial marker tracking software for studying cell mechanics in a three-dimensional environment," SoftwareX **11**, 100417 (2020).

[18]K. Goodarzi and S. S. Rao, "Structurally decoupled hyaluronic acid hydrogels for studying matrix metalloproteinase-mediated invasion of metastatic breast cancer cells," Int J Biol Macromol **277**, 134493 (2024).

[19]C. O. Crosby, A. Hillsley, S. Kumar, B. Stern, S. H. Parekh, A. Rosales, and J. Zoldan, "Phototunable interpenetrating polymer network hydrogels to stimulate the vasculogenesis of stem cell-derived endothelial progenitors," Acta Biomater **122**, 133–144 (2020).

[20]X. Xiao, Z. Huang, X. Jiang, Y. Yang, L. Yang, S. Yang, C. Niu, Y. Xu, and L. Feng, "Facile synthesize of norbornene-hyaluronic acid to form hydrogel via thiol-norbornene reaction for biomedical application," Polymer **245**, 124696 (2022).

[21]Z.-D. Shi, X.-Y. Ji, H. Qazi, and J. M. Tarbell, "Interstitial flow promotes vascular fibroblast, myofibroblast, and smooth muscle cell motility in 3-D collagen I via upregulation of MMP-1," Am J Physiol Heart Circ Physiol **297**, H1225–34 (2009).

[22]W.-H. Guo and Y.-L. Wang, "A three-component mechanism for fibroblast migration with a contractile cell body that couples a myosin II-independent propulsive anterior to a myosin II-dependent resistive tail," Mol Biol Cell **23**, 1657–1663 (2012).

[23]X. Trepat and J. J. Fredberg, "Plithotaxis and emergent dynamics in collective cellular migration," Trends in Cell Biology **21**, 638–646 (2011).

[24]A. Khang, K. Meyer, and M. S. Sacks, "An inverse modeling approach to estimate Three-Dimensional aortic valve interstitial cell stress fiber force levels," J Biomech Eng **145** (2023).

[25]P. Hameed and G. Manivasagam, "An overview of bio-actuation in collagen hydrogels: a mechanobiological phenomenon," Biophysical Reviews **13**, 387–403 (2021).

[26]W. M. Gramlich, I. L. Kim, and J. A. Burdick, "Synthesis and orthogonal photopatterning of hyaluronic acid hydrogels with thiol-norbornene chemistry," Biomaterials **34**, 9803—9811 (2013).

[27]S. Khetan, M. Guvendiren, W. R. Legant, D. M. Cohen, C. S. Chen, and J. A. Burdick, "Degradation-mediated cellular traction directs stem cell fate in covalently crosslinked three-dimensional hydrogels," Nature Materials **12**, 458–465 (2013).

[28]S. Maji and H. Lee, "Engineering hydrogels for the development of Three-Dimensional in vitro models," International Journal of Molecular Sciences **23**, 2662 (2022).

[29]J. Barrasa-Fano, A. Shapeti, J. de Jong, A. Ranga, J. Sanz-Herrera, and H. Van Oosterwyck, "Advanced in silico validation framework for three-dimensional traction force microscopy and application to an in vitro model of sprouting angiogenesis," Acta Biomaterialia **126**, 326–338 (2021).

[30]A. Izquierdo-Álvarez, D. A. Vargas, Á. Jorge-Peñas, R. Subramani, M.-M. Vaeyens, and H. Van Oosterwyck, "Spatiotemporal analyses of cellular tractions describe subcellular effect of substrate stiffness and coating," Annals of Biomedical Engineering **47**, 624–637 (2019).

[31]M. Colasurdo, E. B. Nieves, M. A. Fernández-Yagüe, C. Franck, and A. J. García, "Adhesive peptide and polymer density modulate 3d cell traction forces within synthetic hydrogels," Biomaterials **288**, 121710 (2022).

[32]D. Shakiba, F. Alisafaei, A. Savadipour, R. A. Rowe, Z. Liu, K. M. Pryse, V. B. Shenoy, E. L. Elson, and G. M. Genin, "The balance between actomyosin contractility and microtubule polymerization regulates hierarchical protrusions that govern efficient Fibroblast–Collagen interactions," ACS Nano **14**, 7868–7879 (2020).

[33]M. S. Hall, F. Alisafaei, E. Ban, X. Feng, C.-Y. Hui, V. B. Shenoy, and M. Wu, "Fibrous nonlinear elasticity enables positive mechanical feedback between cells and ecms," Proceedings of the National Academy of Sciences **113**, 14043–14048 (2016), https://www.pnas.org/doi/pdf/10.1073/pnas.1613058113.

[34]S. Hervas-Raluy, M. J. Gomez-Benito, C. Borau-Zamora, M. Cóndor, and J. M. Garcia-Aznar, "A new 3d finite element-based approach for computing cell surface tractions assuming nonlinear conditions," PLoS One **16**, e0249018 (2021).

[35]N. R. Richbourg, M. K. Rausch, and N. A. Peppas, "Cross-evaluation of stiffness measurement methods for hydrogels," Polymer **258**, 125316 (2022).

[36]K. Upadhyay, G. Subhash, and D. Spearot, "Hyperelastic constitutive modeling of hydrogels based on primary deformation modes and validation under 3d stress states," International Journal of Engineering Science **154**, 103314 (2020).

[37]J. D. Berry, M. Biviano, and R. R. Dagastine, "Poroelastic properties of hydrogel microparticles," Soft Matter **16**, 5314–5324 (2020).

[38]J. Wang and J. C. Burton, "Hyperelastic swelling of stiff hydrogels," Phys. Rev. Lett. **134**, 148203 (2025).

[39]M. Eden and H. S. Mahato, "Homogenization of a poroelasticity model for fiber-reinforced hydrogels," Mathematical Methods in the Applied Sciences **45**, 11562–11580 (2022), https://onlinelibrary.wiley.com/doi/pdf/10.1002/mma.8466.

[40]P. Mollenkopf, J. A. Kochanowski, Y. Ren, K. H. Vining, P. A. Janmey, and P. K. Purohit, "Poroelasticity and permeability of fibrous polymer networks under compression," Soft Matter **21**, 2400–2412 (2025).

[41]G. D. Degen, Y.-T. Chen, A. L. Chau, L. K. Månsson, and A. A. Pitenis, "Poroelasticity of highly confined hydrogel films measured with a surface forces apparatus," Soft Matter **16**, 8096–8100 (2020).

[42]D. He and Y. Hu, "Nonlinear visco-poroelasticity of gels with different rheological parts," Journal of Applied Mechanics **87**, 071010 (2020), https://asmedigitalcollection.asme.org/appliedmechanics/article-pdf/87/7/071010/6534920/jam_87_7_071010.pdf.

[43]J. T. Liu, A. K. Glaser, C. Poudel, and J. C. Vaughan, "Nondestructive 3d pathology with light-sheet fluorescence microscopy for translational research and clinical assays," Annual Review of Analytical Chemistry **16**, 231–252 (2023).

[44]E. Jalilian, W. Raimes, and R. M. Macias, "Transcriptional profiling reveals fundamental differences in ips-derived cd34+ cells versus adult circulating cd34+," Peertechz Journal of Biology and Medicine **8(1)**, 001–013 (2024).

[45]A. Khang, Q. Nguyen, X. Feng, D. P. Howsmon, and M. S. Sacks, "Three-dimensional analysis of hydrogel-imbedded aortic valve interstitial cell shape and its relation to contractile behavior," Acta Biomaterialia **163**, 194–

209 (2023), the Mechanics of Cells and Fibers.

[46]S. van der Walt, J. L. Schönberger, J. Nunez-Iglesias, F. Boulogne, J. D. Warner, N. Yager, E. Gouillart, T. Yu, and the scikit-image contributors, "scikit-image: image processing in python," PeerJ **2**, e453 (2014).

[47]P. Cignoni, M. Callieri, M. Corsini, M. Dellepiane, F. Ganovelli, and G. Ranzuglia, "MeshLab: an Open-Source Mesh Processing Tool ," in *Eurographics Italian Chapter Conference*, edited by V. Scarano, R. D. Chiara, and U. Erra (The Eurographics Association, 2008).

[48]F. Pedregosa, G. Varoquaux, A. Gramfort, V. Michel, B. Thirion, O. Grisel, M. Blondel, P. Prettenhofer, R. Weiss, V. Dubourg, J. Vanderplas, A. Passos, D. Cournapeau, M. Brucher, M. Perrot, and E. Duchesnay, "Scikit-learn: Machine learning in Python," Journal of Machine Learning Research **12**, 2825–2830 (2011).

[49]C. Geuzaine and J.-F. Remacle, "Gmsh: A 3-d finite element mesh generator with built-in pre- and post-processing facilities," International Journal for Numerical Methods in Engineering **79**, 1309–1331 (2009), https://onlinelibrary.wiley.com/doi/pdf/10.1002/nme.2579.